### Title
Passive and wireless, implantable glucose sensing with phenylboronic acid hydrogel-interlayer RF resonators




### Authors
Dautta, Manik
Alshetaiwi, Muhannad
Escobar, Jens
et al.



### Publication Date
2020-03-01

### DOI
10.1016/j.bios.2020.112004

Peer reviewed

HHS Public Access

Author manuscript

*Biosens Bioelectron*. Author manuscript; available in PMC 2021 March 01.

Published in final edited form as:

*Biosens Bioelectron*. 2020 March 01; 151: 112004. doi:10.1016/j.bios.2020.112004.

# Passive and wireless, implantable glucose sensing with phenylboronic acid hydrogel-interlayer RF resonators

**Manik Dautta**[a], **Muhannad Alshetaiwi**[a], **Jens Escobar**[b], **Peter Tseng**[a,b,*]

[a]Department of Electrical Engineering and Computer Science, University of California Irvine, Engineering Hall #3110, Irvine, CA, 92697, USA

[b]Department of Biomedical Engineering, University of California Irvine, Engineering Hall #3110, Irvine, CA, 92697, USA

## Abstract

A phenylboronic acid-based, hydrogel-interlayer Radio-Frequency (RF) resonator is demonstrated as a highly-responsive, passive and wireless sensor for glucose monitoring. Constructs are composed of unanchored, capacitively-coupled split rings interceded by glucose-responsive hydrogels. Phenylboronic acid-hydrogels exhibit volumetric and dielectric variations in response to environmental glucose concentrations—these are efficiently converted to large shifts in the resonant response of interlayer-RF sensors. These tiny, stretchable and scalable sensors (5 mm × 5 mm × 250 μm) require no microelectronics or power at the sensing node and can be read-out remotely via near-field coupling. Sensors exhibit high sensitivities (~10% shift in resonant frequency—corresponding to 50 MHz—per 150 mg/dL of glucose), possess a limit of detection of 10 mg/dL, and a step response time of approximately 1 hour to abrupt shifts in carbohydrate concentration. Notably, these sensors exhibited no signal drift or hysteresis over the time periods characterized herein (45 days at room temperature). We transform sensors into bioelectronic RF reporter-tags via the attachment of a single LED—these remotely report on glucose concentration via emitted light. We anticipate the non-degradative, long-term nature of both RF read-out and phenylboronic acid-based hydrogels will enable biosensors capable of long-term, remote read-out of glucose.

### Keywords

glucose sensing; hydrogel sensors; wireless biosensors; wearable biosensors; implantable sensors

*Corresponding author. Department of Electrical Engineering and Computer Science, University of California Irvine, Engineering Hall #3110, Irvine, CA, 92697, USA. tsengpc@uci.edu (P. Tseng).



**Appendix A:** Supplementary material.

## 1. Introduction

Continuous glucose monitors (CGM) represent the modern start-of-the-art treatment of diabetic patients. These devices enable the on-demand measurement of the glucose levels, which can then be accordingly utilized to manage patient blood sugar level. A variety of glucose sensing biosensors have been reported—these can be generally categorized as electrochemical (Karyakin et al., 1995; Bandodkar et al., 2018; Martínez et al., 2019), optical (Hsieh et al., 2004; Barone et al., 2005; Hao et al., 2017), or dielectric (Yilmaz et al., 2019; Huang et al., 2010) sensors. Modern CGM typically relies on the scavenging of electrons from glucose via glucose oxidase (for example the Dexcom CGM or FreeStyle Libre) in electrochemical sensors. These devices are fundamentally limited by the lifetime of glucose oxidase—while a myriad of strategies have been employed to extend sensor lifetime (Kausaite--Minkstimiene et al., 2018; Shamsipur et al., 2010; Tseng et al., 2016), glucose oxidase activity will inevitably degrade over time, and amperometric read-out will eventually lead to signal drift and reference electrode breakdown.

Phenylboronic acid (PBA) hydrogel-based sensors have recently emerged as a viable competitor to enzymatic sensors (an example is the recently FDA-approved Eversense long-term CGM). In contrast to existing CGM that relies on enzymatic activity, PBA-hydrogels reversibly bind to glucose (as well as other sugar molecules) and subsequently swell or deswell (Zhang et al., 2013), and this binding is not subject to degradation (Kim et al., 2018). Thus, it is anticipated that such materials could potentially form the backbone of next-generation, long-term CGM. Various strategies have been employed to convert the behavior of PBA-based, glucose-sensitive hydrogels into usable electronic signals. These include optical (Elsherif et al., 2018; Heo et al., 2011; Gupta et al., 2013), piezoresistive (Baker et al., 2008; Çiftçi et al., 2013), and dielectric Micro-Electro-Mechanical Systems (MEMS)-based techniques (Huang et al., 2010; Lei et al., 2006). Fluorescence-based approaches (whose fluorescent intensity will modulate with hydrogel swelling) have so-far seen the most success *in-vivo* (Heo et al., 2011; Shibata et al., 2010). When implanted, sensors have achieved readout at 5 months (possibly longer). However, these sensors depend on fluorophores that will bleach with repeated illumination (in addition to reduced signal over time due to oxidative processes generated during encapsulation or implantation), and cannot practically be read-out without electronics at the sensing node. This is due to conflicting optical signals from the environment, fluorophore bleaching when exposed to sunlight, and more. In practice, complex electronics and heavy encapsulation at the sensing node are required to achieve consistent readout (Eversense CGM). In addition, these devices are self-limited by the read-out itself, which will degrade fluorescence over time. In general, other optical based approaches—including nanostructured strategies—will see similar issues during implementation in implanted settings (Lee et al., 2004; Xue et al., 2014).

MEMS dielectric sensors present a potentially powerful strategy to transduce signals from PBA-hydrogels. Passive, wireless MEMS-based sensors are utilized in a number of commercial medical devices monitoring the pressure of ventricular arteries(Fonseca et al., 2006) or intraocular pressure (Agarwal et al., 2018). Existing PBA-based MEMS sensors, however, inefficiently convert the signals from the hydrogel to electrical signals (Lei et al., 2006; Huang et al., 2013). These additionally require complex, multi-layer microfabrication

steps, and hydrogels are further encapsulated in mechanically-fixed cavities that prevent the complete swelling response of the hydrogel. Existing studies on PBA-based wireless MEMS sensors interconvert the signal from the hydrogel to pressure (PBA-hydrogels are typically extremely soft), and exhibits minor shifts in resonant frequency (1%) at physiological concentrations of glucose (Lei et al., 2006).

In this publication, we develop a phenylboronic acid-based, passive and wireless sensor for remote glucose monitoring by extending the capabilities of hydrogel-interlayer Radio-Frequency (RF) resonators presented in a recent publication (Tseng et al., 2018). Constructs are composed of unanchored, capacitively-coupled split rings interceded by glucose-responsive hydrogels. This forms highly sensitive sensors that can be read out remotely via inductive coupling with a remote reader/read-out coil. These modernized RF sensors resolve many issues present with existing remote glucose biosensors—they are fully flexible/stretchable for integrability into a multitude of environments, can be read out through opaque mediums, and require no microelectronic components at the sensing node. Importantly, the sensor read-out is non-degradative as no electrolysis and minimal heat is generated during RF read-out. This is in contrast to many optical sensors that utilize degradable transducers, such as fluorescent or colorimetric markers. When combined with hydrogel polymers that are more robust than enzymes, we anticipate PBA-interlayer RF sensors could survive in a variety of environments and facilitate continuous glucose read-out for extended periods of time. Our first generation sensors exhibited zero signal drift and/or degradation of sensor response over the time periods/storage characterized herein (45 days at room temperature with read-out at regular intervals).

## 2. Materials and Methods

### 2.1 Chemicals

Acrylamide and methylene bisacrylamide (PAM), 3-(Acrylamido)phenylboronic acid (PBA), Phosphate Buffered Saline (PBS), Ammonium Persulfate (APS) and N,N,N`,N`-Tetramethyl-ethylenediamine (TEMED), D-(+)-Glucose, D-(−)-Fructose all are purchased from Sigma Aldrich. D-galactose and Lactose are purchased from Fisher Scientific. All chemicals are used without further modification.

### 2.2 Fabrication

Resonator patterns were designed using 2D design tools. Metal conductive sheets (aluminum or titanium foil) were pasted on vinyl, and conductive patterns were created using an electronic cutter (Silhouette Cameo 3). A known amount of hydrogel precursor solution was deposited above one half of the resonator (corresponding to the desired hydrogel thickness) before the second half of the resonator was aligned and set above the hydrogel interlayer. This gelation proceeded in a 3-dimensional PDMS (SYLGARDTM 184, Silicone Elastomer; Base: Curing Agent=10:1) mold. After the hydrogel was polymerized at room temperature, the sensor was demolded in acetone to release it from the vinyl and kept in the Phosphate Buffered Saline (ionic strength: 35 mM) 1 day before experiments. The schematic representation of the fabrication technique is included in Suppl. Figure S1.

### 2.3 p(PBA-*co*-AAm) Hydrogel Synthesis

Two stock solution of 20% PAM (composed of 20% w/w acrylamide, and 6% (w/w) methylene bis acrylamide in DI, Sigma), and 0.32 M PBA in 53.85% ethanol were initially prepared. Appropriate amounts of the two stock solutions (20% PAM: 0.32 M PBA = 8:9 for our final hydrogel) were mixed in a microcentrifuge tube, followed by addition of 0.15% (w/w) APS and 0.5% (v/v) TEMED to synthesize a 23.5% PBA functionalized 4% PAM hydrogel (p(PBA-*co*-AAm)).

### 2.4 *In-Vitro* Validation

Resonant responses of the antennas were characterized with a Keysight E5063A network analyzer using an RF Explorer H-loop antenna attached to the coaxial input. 5mm × 5mm × 250μm interlayer structures were placed on a plastic petri dish for measurements. For characterization, the infiltration/release rate of the sensors, each sensor was exposed to a set concentration of 200 mg/dL in PBS (35mM ionic strength, pH=7.4). For the average response, three sets of three sensors were exposed to the respective analyte solution of 200 mg/dL concentration for four hours. For incremental response, the concentration of the solution was increased nine times by 50 mg/dL (0 to 400 mg/dL), and in each step the sensor was monitored over three hours. For the repeatability response, sensors were measured after four hours exposure to 200 mg/dL solution and reset to initial state overnight for 10 trials. In all experiments solutions were initially mixed via a 5 to 10 second pipetting of a high concentration glucose dose that would dilute to yield the desired glucose concentration. Otherwise the solution was stagnant and unagitated. Some basic performance parameters (including the consistency/repeatability of the response) are presented in the Suppl. Table S1.

### 2.5 Glucose RF reporter-tags

For wireless power transfer, a miniVNA Tiny was used as a signal generator, and a 20dB gain power amplifier was used to amplify the signal. For light intensity measurements, light illuminance variations were measured in a semi-dark room using a REED R8140 LED Light Meter for a 2cm × 2cm × 500μm sensor initially operating at 96MHz (generated signal frequency was 116MHz). To test the response of the sensor circuit, the light illuminance was monitored while glucose concentration was stepped up by 200 mg/dl. The light intensity over 10 seconds was averaged every 5 minutes over the experimental duration.

### 2.6 *Ex vivo* Validation

Chicken and pork were washed in phosphate buffered saline three times over 5 days before sensors were implanted right under the outer skin. Next, they were exposed to two concentrations of glucose (0 and 500mg/dL) while measurements were taken remotely by a network analyzer. For long term studies, sensors were tested for response to a step change of 200 mg/dL glucose over 3 hours at every 3$^{rd}$ day. This experiment proceeded over 45 days..

## 3. Results and Discussion

In this publication, we demonstrate a facile, inexpensive strategy of generating passive and wireless RF sensors (Tseng et al., 2018) that are highly responsive to shifts in glucose. A

diagram of the working components of the final sensor is shown in Figure 1a, which consists of 2 elements, a metal conductor and glucose sensitive hydrogel (although one side of the sensor is typically affixed to a thin vinyl sheet to facilitate manipulation). A p(PBA-*co*-AAm) hydrogel bilayer intercedes two split ring resonators that are unanchored and free to move. In brief, PBA-hydrogels operate as follows: at a certain pH range (around 6.5 to 8.5 depending on exact molar chemistry), PBA readily reacts to available hydroxide ions that convert PBA into more negatively charged molecules. Cis-diols, like sugar molecules, can then bind with this boronate complex and stabilize its charged form. This binding manifests as either a 1:1 monobidentate complex that leads to hydrogel swelling, or a 2:1 bis-bidentate complex that leads to hydrogel contraction (Zhang et al., 2013). PBA-hydrogels generally behave in one of two ways (Zhang et al., 2013). In the first type, the hydrogel will transition from swelling to deswelling, and finally swelling again with increasing concentrations of glucose—this occurs because binding kinetics at moderate concentration favors the deswelling 2:1 complex, whereas at higher concentrations will transition back to the swelling 1:1 complex. In the second type, the hydrogel will generally only swell with increasing glucose. In this publication, we utilize a polyacrylamide-based PBA-hydrogel that primarily swells with increasing glucose concentration over the typical working range of glucose sensors (Elsherif et al., 2018; Lin et al., 2010; Siegel et al., 2010; Zhang et al., 2012). Polyacrylamide forms well-behaved, tunable hydrogels that are generally accepted for use in biomedical applications (El-Sherbiny and Yacoub, 2013). Such properties make them suitable for glucose sensors. Of note for PBA-hydrogels, in glucose-dominated environments (such as blood), hydrogel swelling becomes directly correlated with glucose concentrations. In addition, these materials typically require dosing with dexamethasone to prevent inflammation.

A simplified lumped element model of our RF biosensor is shown in Figure 1b, which can be approximated as an RLC equivalent circuit. The PBA-based hydrogel swells in the presence of glucose, which will modulate the thickness of the capacitor formed by coupling the two split rings. The swelling of the hydrogel in this construct directly couples to the capacitance of the resonator, and thus its resonant frequency ($f_{res} = \frac{1}{2\pi\sqrt{L_S C}}$). This resonant response of the sensor can then be read out remotely using a vector network analyzer (we typically use either a benchtop—Keysight—or compact—miniVNA—iterations of these).

In general, analytical RF sensors need to operate at around 1 GHz and below. Operation at such frequencies facilitates sensor read-out by giving access to portable network analyzers and UHF RFid readers. In addition, water begins to heavily absorb RF signals at 1 GHz and above—sensors operating above these frequencies cannot be implanted too deep in tissue. We were able to obtain electrically-small sensors shown in Figure 1c (~5mm × 5mm) operating at below 1 GHz using simple fabrication steps (Kao et al., 2016; Kim et al., 2016) and sacrificial release techniques (Tseng et al., 2014) (Suppl. Figure S1). Conductive split rings were separately patterned using a vinyl cutter, and silanized to facilitate covalent bonding to metal. Hydrogel precursor of a known volume is drop-cast above one of the split rings and allowed to gel before the opposing split ring is set above the precursor solution. Either one or both vinyl backing layers are finally removed from the sample using acetone. Sensors can be tuned to a wide variety of sizes and operating frequencies by modulating the

size of the sensor or the thickness of the hydrogel interlayer (Figure 1d and e). Typically, passive sensors possessing sub-GHz operation require either a large areal footprint, microfabrication to generate high inductance planar coils, and/or integrated microelectronics. The low operating frequencies, small size, and inexpensive nature of our RF sensors were facilitated by both the broad-side coupling of the resonator, as well as to the high dielectric constant of hydrogel (close to 80). As synthesized, the resonant frequency of sensors was slightly lower than the frequency after sensors were equilibrated in their final working solution (PBS, pH=7.4, ionic strength=35 mM), indicative of minor swelling in the hydrogel during this process (Suppl. Figure S2). We anticipate utilizing this format of glucose/carbohydrate biosensor in a variety of biofluids (such as saliva, urine, sweat, or blood), or in unique avenues such as food or culture medium monitoring. Such fluids exhibit a wide variety of ionic strengths, from low (0 mM in many drinks), to moderate (~20 mM in sweat, urine, or saliva), to high (~150 mM in blood). For the purposes of this publication, we chose to optimize our sensors at a moderate ionic strength (~35 mM). This is above the ionic strength of many relevant fluids that could be monitored, but below that of blood. We studied the magnitude read-out of our sensors while operating at this ionic strength versus that of solutions similar to blood (Suppl. Figure S3). Our sensors generally exhibited a magnitude of ~5.5 dB at our test conditions of 35 mM, and exhibit a minor drop to ~3 dB at 150 mM—the resonant frequency of the sensors remains readable at both these conditions. While the read-out of sensor resonant frequency remains adequate at higher ionic strength solutions, the reduced quality factor (Q) of the sensor indicates that it would be more difficult to resolve very small shifts in glucose. If extremely high sensitivities are required, we anticipate that the utilization of modern approaches in materials science (i.e. encapsulation/integration with salt suppressing hydrogels such as polyacrylic acid (Zhu et al., 2019) or chitosan (Sapna et al., 2019)), or electromagnetic amplification (via exceptional points of degeneracy) (Kazemi et al., 2019), will dramatically improve sensor sensitivities.

We ran a series of studies to optimize the performance of our sensor. This occurred both by directly studying the swelling of a PBA hydrogel block, as well as tracking sensor behavior for different sizes and thicknesses of the hydrogel interlayer. Mass transport of glucose into our sensor was improved by removing vinyl backing layers and introducing bypass holes into metal conductors (Suppl. Figure S4). Our data additionally revealed that the smaller (5 mm × 5 mm) and thinner (250 μm) hydrogel interlayers can swell much faster than their larger (1 cm × 1 cm) and thicker (500 μm) counterparts (Suppl. Figure S5). These results indicate that hydrogel structural rearrangement is the limiting factor for sensor response time, and further reducing of hydrogel volume will yield quicker and more responsive sensors. The swelling of the hydrogel dependeds on the pH of the environment, with hydrogel swelling exhibiting an optimal sensitivity at around pH 7 to 7.5 (Suppl. Figure S6). Percent mass of the polymer similarly has an effect on the swelling—we found that lower percent mass of the polymer will exhibit enhanced swelling, however, these will require slightly more time to saturate (Suppl. Figure S7). In this case, we believe the lower elastic modulus of the lower percent mass polymer enables a more responsive sensor. While sensors could potentially be further tuned, we settled on 5 mm × 5 mm sensors with a 250 μm thick interlayer of 4% polyacrylamide. These sensors exhibited adequate response times and resonant shifts (Suppl. Figure S8) for measurement of hourly oscillations in glucose at room

temperature. This response rate will vary with temperature, and response times ~4 to 5 fold faster have been found at elevated temperatures (37° C) as opposed to room temperature (Tierney et al., 2009).

For glucose, association constants with boronate complexes have been measured to be extremely fast with $k_{on}$ =.6 $M^{-1}$ $s^{-1}$, and $k_{off}$ = .13 $M^{-1}$ $s^{-1}$ (Ni et al., 2012). In addition, the diffusion speed of glucose into hydrogel has been estimated at close to 10 s for 100 μm-thick hydrogels (Ben-Moshe et al., 2006). Both of these are significantly faster than the response time of most synthesized hydrogels. In general, it appears the thickness/density of the hydrogel limits the response time of sensors (which was found and documented in our studies). For example, 1 to 5 mm thick hydrogels have been reported to exhibit very slow response times of 400 minutes and greater (Matsumoto et al., 2004). The thickness of our hydrogels (250 to 400 μm) are similar with recently published work on optical diffusers based on PBA hydrogels (Elsherif et al., 2018)—these exhibited similar response times to our sensors (60 minutes). Ultrathin hydrogel films on the micrometer scale (and using a similar hydrogel formulation of acrylamide-PBA) exhibited 5 minute response times (Zhang et al., 2012). Thinner and lower density hydrogels lead to more rapid response times. In the future, we anticipate utilizing much thinner hydrogel films to obtain higher sensitivities and quicker response times.

We studied the response of our sensors to a variety of carbohydrates purported to induce changes in the osmotic swelling of phenylboronic acid-based hydrogels, including glucose, galactose, fructose, and lactose (Figure 2 and Suppl. Figure S9). We first analyzed the temporal response of sensors to a relatively large shock in carbohydrate concentration of 200 mg/dL of respective carbohydrates (Figure 2d–f). All sensors reached within 80% of their final response within approximately 1 hour, which is satisfactory for measuring hourly oscillations in glucose (these sensors will respond slower or faster depending on environmental temperature). The response time of our sensors was found to be 56 minutes for 50 mg/dL, 63 minutes for 100 mg/dL, 70 minutes for 200 mg/dL, and 85 minutes for 500 mg/dL of glucose. While the sensor's response to galactose and fructose would smoothly saturate to its final value, we found that the sensor response to glucose would often exhibit a minor initial overshoot of its final response, indicating some additional complexity in the kinetics of the osmotic swelling of our p(PBA-co-Aam) in glucose. Additionally, we found that while glucose would release from the hydrogel relatively quickly, galactose exhibited a much slower release, and a percentage of fructose remained permanently trapped in the PBA hydrogel (this would be later confirmed in the response of our sensors to repeated stimuli). In general, we believe the ability of our sensors to continuously and readily resolve the kinetics of hydrogel swelling may additionally be utilized to optimize and/or screen for novel polymer combinations.

Next, we performed a test on the average response of a triplicate set of sensors produced from a single batch using the same exact conditions (polymer concentrations, infiltrated volume, etc.). Note that we found that there was minor batch-to-batch variation in the response of sensors. This is due to the difficulty in controlling the exact polymer concentration and polymerization conditions between different batches in an academic setting that utilizes small volumes and imperfect environmental conditions. Nevertheless, we

found sensors built from the same batch to exhibit consistent resonant peaks and shifts in various carbohydrates (Figure 2g–i). As with literature, we found that swelling exhibited an ordering that followed published results, where fructose>galactose>glucose>lactose. (Nguyen et al., 2012; Xu et al., 2019) Lactose exhibited very minor shifts in resonant frequency that were difficult to measure (Suppl. Figure S9).

Furthermore, we performed studies on the step and repeatability response of our sensors to glucose, galactose, and fructose (Figure 2j–o). The step responses clearly indicate the primary response shift in resonance frequency occurs within around an hour and remains constant after thisafterwards. For the repeatability esperiment, the sensor response to glucose and galactose at 200 mg/dL was repeatable and indicated no retention of carbohydrate in the hydrogel—note that in these repeat studies 1 day was given for samples to rest that allowed the galactose to fully exit the hydrogel. The sensor baseline shifted in fructose, however, indicating that a percent of fructose becomes permanently complexed to the phenylboronic acids in the gel. This fixed percent appears constant for extended repeated stimuli at this initial stimulation concentration. Additionally, the suitability of the sensor to track glucose in glucose dominated environments (such as in interstitial fluids whose glucose concentration is 130 mg/dL and fructose concentration is 0.1 mg/dL) was studied in an interference experiment (Suppl. Figure S10).

Next, we perform an analysis of the sensitivity of the sensors extracted from the resonant frequency and magnitude response in various concentrations of glucose, galactose, and fructose (Figure 3a–c). Sensors exhibited initial linearity in frequency shift with respect to concentration shifts, possessing rates of 304 KHz/(mg/dL), 540 KHz/(mg/dL), and 2.804 MHz/(mg/dL) for glucose, galactose, and fructose respectively (Figure 3d–f). These shifts in resonant frequency mute somewhat at higher carbohydrate concentrations (above 150 mg/dL for glucose). We also found that the magnitude of the sensor response was additionally indicative of carbohydrate concentration, with resonant response to glucose, galactose, and fructose all exhibiting initially improved Q with increasing carbohydrate concentration (Figure 3g–i and Suppl. Figure. S9). This is somewhat counterintuitive because a swollen interlayer implies a greater presence of water and salt that would increase the dielectric loss of the hydrogel (this ends up being true for fructose that swells heavily). However, the formation of the boronate-carbohydrate complexes seems to suppress mobile ion concentration during moderate swelling, thus in fact increasing the Q of the resonator during swelling. This is suggestive that further manipulation in the hydrogel chemical composition may be a simple route to improve the resonant behavior of the sensor. As a special note, as shown in Figure 3i, the Q the resonator response to high fructose concentrations does eventually reduce—it appears that for fructose the exceptionally heavy swelling of the sensor (increasing the interlayer thickness significantly and reducing sensor magnitude) becomes the dominant response over the suppression of mobile ions.

We next created facile light-up RFid sensor-circuits that could report on environmental glucose concentration through the intensity of light. This was executed by utilizing context-dependent wireless power transfer via inductive coupling between an active source and our glucose-dependent, passive LC resonator (Figure 4a). Wireless power is initially coupled into our RF sensor with a single LED attached across the ends of a single split ring (Figure

4b). The frequency of this power is tuned to be above the resonant frequency of the sensor so that as the sensor swells and shifts to a higher frequency due to the presence of glucose, the transmitted power will more efficiently transfer into the circuit. This type of scheme can be read-out through transparent or partially transparent layers (in this case pig skin). As shown in Figure 4c, LED illuminance can be readily visualized through thin biological constructs. Additionally, LED illuminance correlated strongly with the resonant behavior of the sensor (Figure 4d). As the sensor responds to a step concentration of glucose (500 mg/dL), the illuminance of our sensor-circuit increases linearly before nearing saturation at the 1 hour mark (as is the response time of these sensors at room temperature). This scheme simplifies the read-out of these sensors—a benchtop or portable vector network analyzer is no longer required to read-out sensors, rather a simple power amplifier circuit and camera (for example on a cellphone) can be used to determine glucose concentration. We anticipate that, in this vein, our passive and wireless sensors can be utilized as a powerful component with a myriad of bioelectronic systems and schemes.

We performed a small set of preliminary studies seeking to display the utility of our sensors, and its potential to be utilized in implantable settings (such as alongside biological components, Figure 5a). We first attempted to verify that our sensor could be read when implanted alongside or within biological constructs. Such structures possess complex moieties (such as fats, protein, water, and muscle) that could potentially absorb or scatter Radio-Frequency signals and disrupt sensor read-out. In general, however, biological constructs possess minimal absorbance in the MHz frequency range (Barba and d'Amore, 2012; Vollmer, 2003), and it should be expected that these electrically-small sensors could be read-out without issues. We implanted sensors *ex-vivo* below the skin of a chicken and pig meat and tested the read-out of our sensors (25 $mm^2$ and 100 $mm^2$) to step concentration increases of 500 mg/dL of glucose (Figure 5b and Suppl. Figure S11). This scenario is meant to mimic the measurement of glucose in interstitial fluid right below the outer layer of skin (and similar to the FreeStyle Libre or Eversense CGM). Sensors behaved similar to *in-vitro* settings, with smaller sensors exhibiting a much faster response (nearly saturating within 1 hour), while larger 100 $mm^2$ sensors took significantly longer to respond fully (3 hours).

Lastly, we performed preliminary studies on the potential of this strategy for long-term readout of glucose (Figure 5c). Phenylboronic acid hydrogels can potentially be used for continuous and long-term glucose sensing, but the read-out must be non-destructive to truly obtain long-term sensing. RF read-out generates no destructive electrolysis, and the minimal heat generated during read-out pulses can be readily buffered by the aqueous environment of these sensors. In this case, the only potential failure mechanism is delamination between metal and hydrogel that can be prevented by silanization treatment of the surface (Yuk et al., 2016). We tested the average response of two sensors exposed to a step of 200 mg/dL glucose concentration. Similar to repeat studies, the sensors response to glucose infiltration and release over 45 days shows consistent reversibility of the sensors without any issues—no delamination of the structure or no retention of glucose in the hydrogel. Importantly, we noticed little to no signal or response drift past the initial week (potentially caused by residual monomer that eventually leached from the hydrogel), indicating that this technique can potentially be used for calibration free, long-term sensing of glucose.

## 4. Conclusions

We have demonstrated a highly-responsive and inexpensive, passive and wireless RF sensor for continuous glucose monitoring. We obtained electrically-small glucose biosensors (~5 mm × 5 mm) operating in sub-GHz regime by using the broad-side coupling of interlayer-RF resonators and high dielectric constant of PBA hydrogel (~80). We believe the combination of non-destructive read-out of RF sensors and robust response of PBA hydrogels may create long-lasting, remote glucose sensors. This is supported by the fact that our sensors exhibited no signal or response drift over characterized time periods (45 days). We anticipate the PBA-hydrogel interlayer can be tuned in thickness or composition to improve sensor response time and sensitivity at physiological conditions. Such passive and wireless sensors could potentially be placed in diverse settings without worry of microelectronic failure/leakage.

## Supplementary Material

Refer to Web version on PubMed Central for supplementary material.

## Acknowledgements

The authors acknowledge funding from the UCI Department of EECS Startup Funds and the Samueli Early Career Faculty Development Award. This research was funded in part by the National Institutes of Health through award R21CA239249.

## References

Agarwal A, Shapero A, Rodger D, Humayun M, Tai Y-C, Emami A, 2018 2018 IEEE Custom Integrated Circuits Conference (CICC). IEEE, pp. 1–4.

Baker GA, Desikan R, Thundat T, 2008 Anal. Chem 80, 4860–4865. 10.1021/ac702588b [PubMed: 18522434]

Bandodkar AJ, Imani S, Nuñez-Flores R, Kumar R, Wang C, Mohan AMV, Wang J, Mercier PP, 2018 Biosensors and Bioelectronics 101, 181–187. 10.1016/j.bios.2017.10.019 [PubMed: 29073519]

Barba AA, d'Amore M, 2012 Microwave Materials Characterization. 10.5772/51098

Barone PW, Baik S, Heller DA, Strano MS, 2005 Nature Mater 4, 86–92. 10.1038/nmat1276 [PubMed: 15592477]

Ben-Moshe M, Alexeev VL, Asher SA, 2006 Anal. Chem 78, 5149–5157. 10.1021/ac060643i [PubMed: 16841941]

Çiftçi H, Tamer U, Teker MŞ, Pekmez NÖ, 2013 Electrochimica Acta 90, 358–365. 10.1016/j.electacta.2012.12.019

El-Sherbiny IM, Yacoub MH, 2013 Glob Cardiol Sci Pract 2013, 316–342. 10.5339/gcsp.2013.38 [PubMed: 24689032]

Elsherif M, Hassan MU, Yetisen AK, Butt H, 2018 ACS Nano 12, 2283–2291. 10.1021/acsnano.7b07082 [PubMed: 29529366]

Fonseca MA, Allen MG, Kroh J, White J, 2006 Tech. Dig. Solid-State Sensor, Actuator, and Microsystems Workshop (Hilton Head 2006). pp. 37–42.

Gupta VK, Atar N, Yola ML, Eryilmaz M, Torul H, Tamer U, Boyaci İH, Üstündağ Z, 2013 Journal of Colloid and Interface Science 406, 231–237. 10.1016/j.jcis.2013.06.007 [PubMed: 23816220]

Hao N, Zhang X, Zhou Z, Qian J, Liu Q, Chen S, Zhang Y, Wang K, 2017 Sensors and Actuators B: Chemical 250, 476–483. 10.1016/j.snb.2017.05.003

Heo YJ, Shibata H, Okitsu T, Kawanishi T, Takeuchi S, 2011 PNAS 108, 13399–13403. 10.1073/pnas.1104954108 [PubMed: 21808049]

Hsieh HV, Pfeiffer ZA, Amiss TJ, Sherman DB, Pitner JB, 2004 Biosensors and Bioelectronics 19, 653–660. 10.1016/S0956-5663(03)00271-9 [PubMed: 14709382]

Huang X, Li S, Davis E, Li D, Wang Q, Lin Q, 2013 J Microelectromech Syst 23, 14–20. 10.1109/JMEMS.2013.2262603 [PubMed: 24511215]

Huang X, Li S, Schultz JS, Wang Q, Lin Q, 2010 Appl. Phys. Lett 96, 033701 10.1063/1.3291669

Kao H.-L. (Cindy), Holz C, Roseway A, Calvo A, Schmandt C, 2016 Proceedings of the 2016 ACM International Symposium on Wearable Computers, ISWC '16. ACM, New York, NY, USA, pp. 16–23. 10.1145/2971763.2971777

Karyakin AA, Gitelmacher OV, Karyakina EE, 1995 Anal. Chem 67, 2419–2423. 10.1021/ac00110a016

Kausaite-Minkstimiene A, Glumbokaite L, Ramanaviciene A, Dauksaite E, Ramanavicius A, 2018 Electroanalysis 30, 1642–1652. 10.1002/elan.201800044

Kazemi H, Hajiaghajani A, Nada MY, Dautta M, Alshetaiwi M, Tseng P, Capolino F, 2019 arXiv:1909.03344 [physics].

Kim A, Lee H, Jones CF, Mujumdar SK, Gu Y, Siegel RA, 2018 Gels 4, 4 10.3390/gels4010004

Kim Jeonghyun, Salvatore GA, Araki H, Chiarelli AM, Xie Z, Banks A, Sheng X, Liu Y, Lee JW, Jang K-I, Heo SY, Cho K, Luo H, Zimmerman B, Kim Joonhee, Yan L, Feng X, Xu S, Fabiani M, Gratton G, Huang Y, Paik U, Rogers JA, 2016 Science Advances 2, e1600418 10.1126/sciadv.1600418 [PubMed: 27493994]

Lee Y-J, Pruzinsky SA, Braun PV, 2004 Langmuir 20, 3096–3106. 10.1021/la035555x [PubMed: 15875835]

Lei M, Baldi A, Nuxoll E, Siegel RA, Ziaie B, 2006 Diabetes Technology & Therapeutics 8, 112–122. 10.1089/dia.2006.8.112 [PubMed: 16472058]

Lin G, Chang S, Hao H, Tathireddy P, Orthner M, Magda J, Solzbacher F, 2010 Sensors and Actuators B: Chemical 144, 332–336. 10.1016/j.snb.2009.07.054

Martínez F, Cifuentes M, Tapia JC, Nualart F, 2019 J Mol Med 97, 1085–1097. 10.1007/s00109-019-01799-5 [PubMed: 31129757]

Matsumoto A, Kurata T, Shiino D, Kataoka K, 2004 Macromolecules 37, 1502–1510. 10.1021/ma035382i

Nguyen QH, Ali M, Neumann R, Ensinger W, 2012 Sensors and Actuators B: Chemical 162, 216–222. 10.1016/j.snb.2011.12.070

Ni N, Laughlin S, Wang Y, Feng Y, Zheng Y, Wang B, 2012 Bioorg Med Chem 20, 2957–2961. 10.1016/j.bmc.2012.03.014 [PubMed: 22464680]

Sapna, Sharma R, Kumar D, 2019 Chapter 29 - Chitosan-Based Membranes for Wastewater Desalination and Heavy Metal Detoxification, in: Thomas S, Pasquini D, Leu S-Y, Gopakumar DA (Eds.), Nanoscale Materials in Water Purification, Micro and Nano Technologies. Elsevier, pp. 799–814. 10.1016/B978-0-12-813926-4.00037-9

Shamsipur M, Najafi M, Hosseini M-RM, 2010 Bioelectrochemistry 77, 120–124. 10.1016/j.bioelechem.2009.07.007 [PubMed: 19674943]

Shibata H, Heo YJ, Okitsu T, Matsunaga Y, Kawanishi T, Takeuchi S, 2010 PNAS 107, 17894–17898. 10.1073/pnas.1006911107 [PubMed: 20921374]

Siegel RA, Gu Y, Lei M, Baldi A, Nuxoll EE, Ziaie B, 2010 J Control Release 141, 303–313. 10.1016/j.jconrel.2009.12.012 [PubMed: 20036310]

Tierney S, Falch BMH, Hjelme DR, Stokke BT, 2009 Anal. Chem 81, 3630–3636. 10.1021/ac900019k [PubMed: 19323502]

Tseng P, Napier B, Garbarini L, Kaplan DL, Omenetto FG, 2018 Advanced Materials 30, 1703257.

Tseng P, Perotto G, Napier B, Riahi P, Li W, Shirman E, Kaplan DL, Zenyuk IV, Omenetto FG, 2016 Advanced Electronic Materials 2, 1600190 10.1002/aelm.201600190

Tseng P, Pushkarsky I, Di Carlo D, 2014 PLoS One 9, e106091. [PubMed: 25153326]

Tsujimoto M, Yabutani T, Sano A, Tani Y, Murotani H, Mishima Y, Maruyama K, Yasuzawa M, Motonaka J, 2007 Analytical Sciences 23, 59–63. 10.2116/analsci.23.59 [PubMed: 17213625]

Vollmer M, 2003 Phys. Educ 39, 74–81. 10.1088/0031-9120/39/1/006

Xu S, Sedgwick AC, Elfeky SA, Chen W, Jones AS, Williams GT, Jenkins ATA, Bull SD, Fossey JS, James TD, 2019 Front. Chem. Sci. Eng 10.1007/s11705-019-1812-5

Xue F, Meng Z, Wang F, Wang Q, Xue M, Xu Z, 2014 Journal of Materials Chemistry A 2, 9559–9565. 10.1039/C4TA01031K

Yilmaz T, Foster R, Hao Y, 2019 Diagnostics 9, 6 10.3390/diagnostics9010006

Yuk H, Zhang T, Lin S, Parada GA, Zhao X, 2016 Nature materials 15, 190. [PubMed: 26552058]

Zhang C, Losego MD, Braun PV, 2013 Chem. Mater 25, 3239–3250. 10.1021/cm401738p

Zhang X, Guan Y, Zhang Y, 2012 Biomacromolecules 13, 92–97. 10.1021/bm2012696 [PubMed: 22136353]

Zhu W, Zhang Y, Wang P, Yang Z, Yasin A, Zhang L, 2019 Materials (Basel) 12 10.3390/ma12040596

## Highlights

New, highly-responsive passive and wireless sensor for continuous glucose monitoring

Tiny glucose biosensor (5 mm × 5 mm × 250 μm) can be readout remotely with any microelectronics at the sensing node

Biosensors exhibits high sensitivities (~10% shift in resonant frequency—corresponding to 50 MHz—per 150 mg/dL of glucose), and a limit of detection of 10 mg/dL.

No signal drift or hysteresis over the multiple low-high glucose cycles and time periods characterized herein (45 days at room temperature), and exhibits a response time of 60 minutes to step shifts in glucose.

Resonators are transformed into glucose-sensing RF reporter tags that light up with increasing glucose concentration.

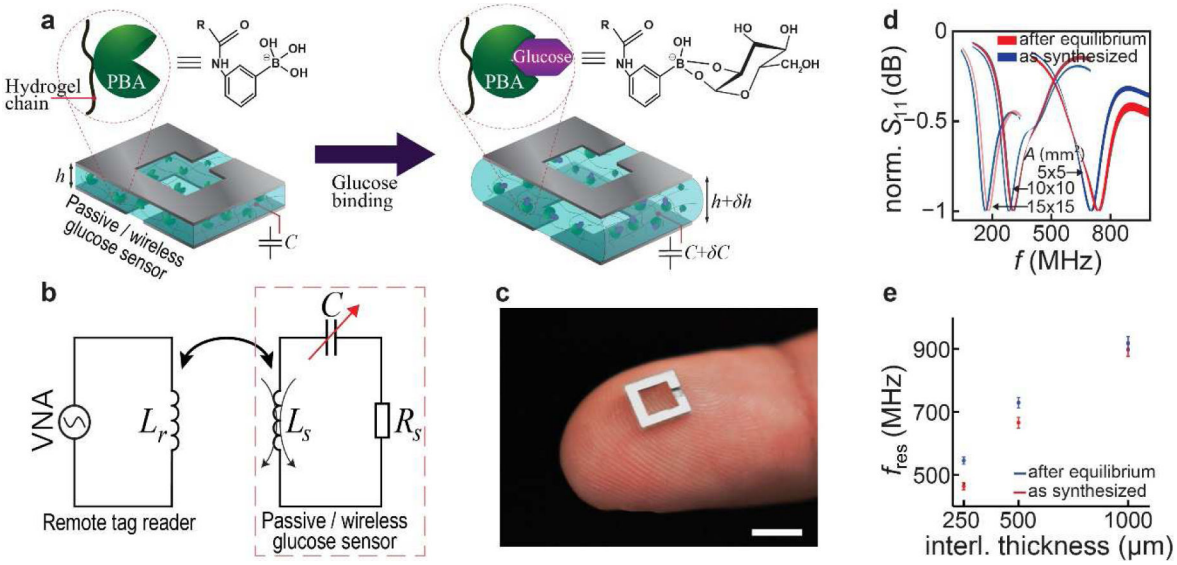


**Figure 1. PBA hydrogel-interlayer RF resonators.**

**(a)** Schematic of glucose binding with Phenylboronic acid (PBA) (top). Schematic of the broad-side coupled, split-ring resonator interceded by p(PBA-*co*-AAm) hydrogel interlayer (bottom). Glucose binding with PBA makes the hydrogel to swell. This modulation in the thickness of the interlayer, in turn, changes the capacitance of the resonator. **(b)** Simplified RLC circuit model for the interlayer-RF sensor and its remote readout system. Change in capacitance will be reflected in the change of the resonant frequency of the sensor. **(c)** Tiny, passive sensors were fabricated using a cheap and simple fabrication technique that requires no microfabrication. Scale bar is 5 mm. **(d-e)** Tunable operating frequency by facile scaling of the size of the structure and thickness of the interlayer hydrogel (N=6, standard deviation (SD)=9.3 MHz).

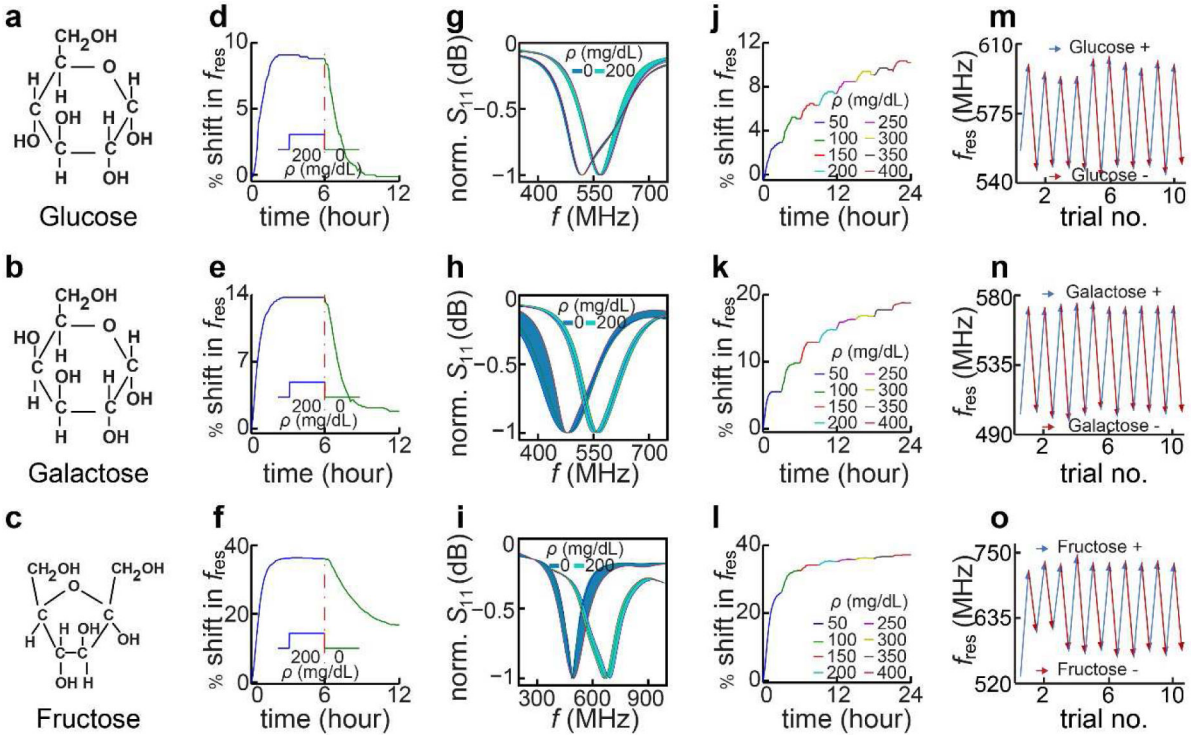


**Figure 2.** ***In-vitro*** **response of phenylboronic acid-based hydrogel-interlayer sensors due to shifts in carbohydrate concentration.**

**(a)-(c)** Schematic of glucose, galactose, and fructose chemical structure. **(d)-(f)** Temporal response of infiltration and release of glucose, galactose and fructose sensors. **(g)-(i)** Average (N=3) response of glucose, galactose and fructose sensors. **(j)-(l)** Incremental step response of glucose, galactose and fructose sensors **(m)-(o)** Repeatability response of sensor to glucose, galactose and fructose (200 mg/dL).

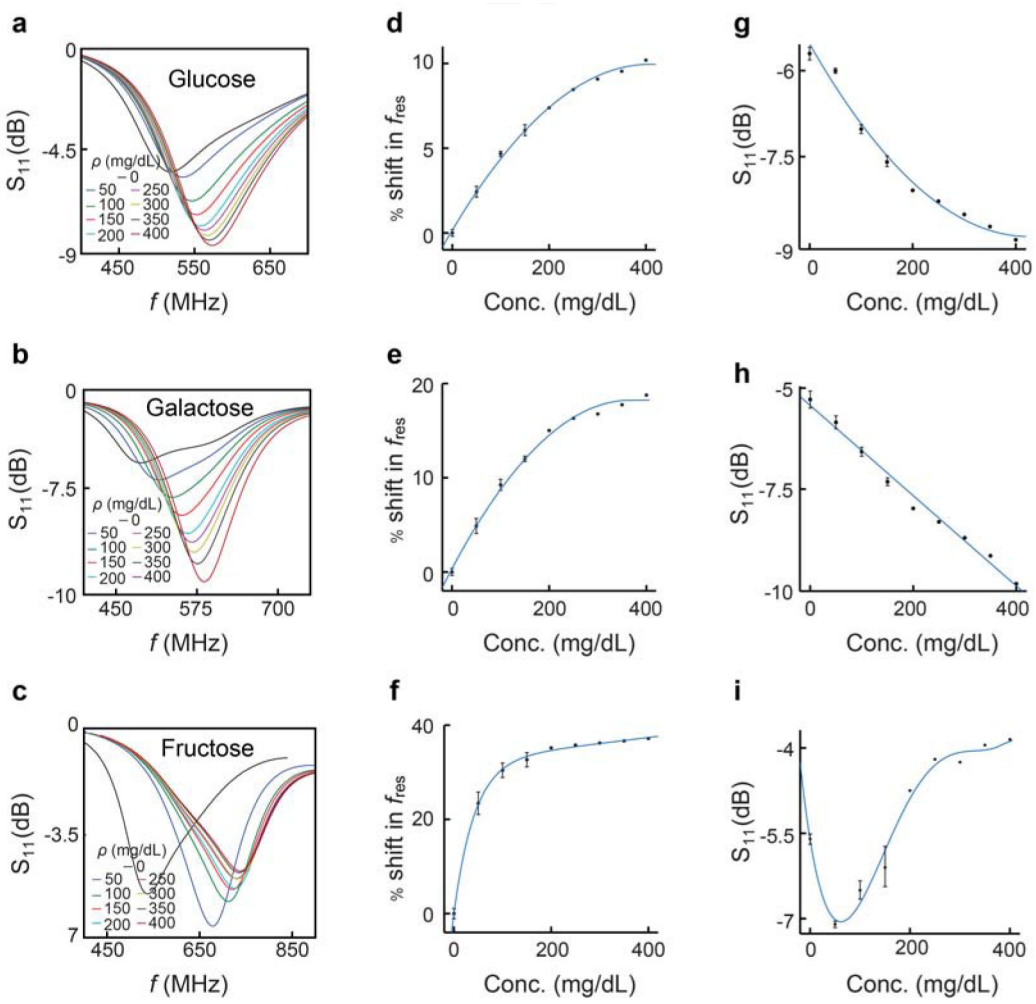


**Figure 3. Extraction of sensor sensitivity from resonant frequency and magnitude.**

**(a)-(c)** Un-normalized spectral response of PBA-interlayer sensors to glucose, galactose, and fructose. **(d)-(f)** Extracted percentage shift in the resonant frequency of sensors as a function of increasing concentration of glucose, galactose, and fructose (N=3, SD=2.07 MHz, 3.65 MHz and 11.85 MHz respectively). **(g)-(i)** Extracted magnitude shift in sensor response to increasing concentration of glucose, galactose and fructose (N=3, SD=0.2 dB, 0.45 dB and 1.2 dB respectively). Note that sensor response was measured in triplicate for their response to the initial four concentrations, before a single sensor was selected to complete the experiment.

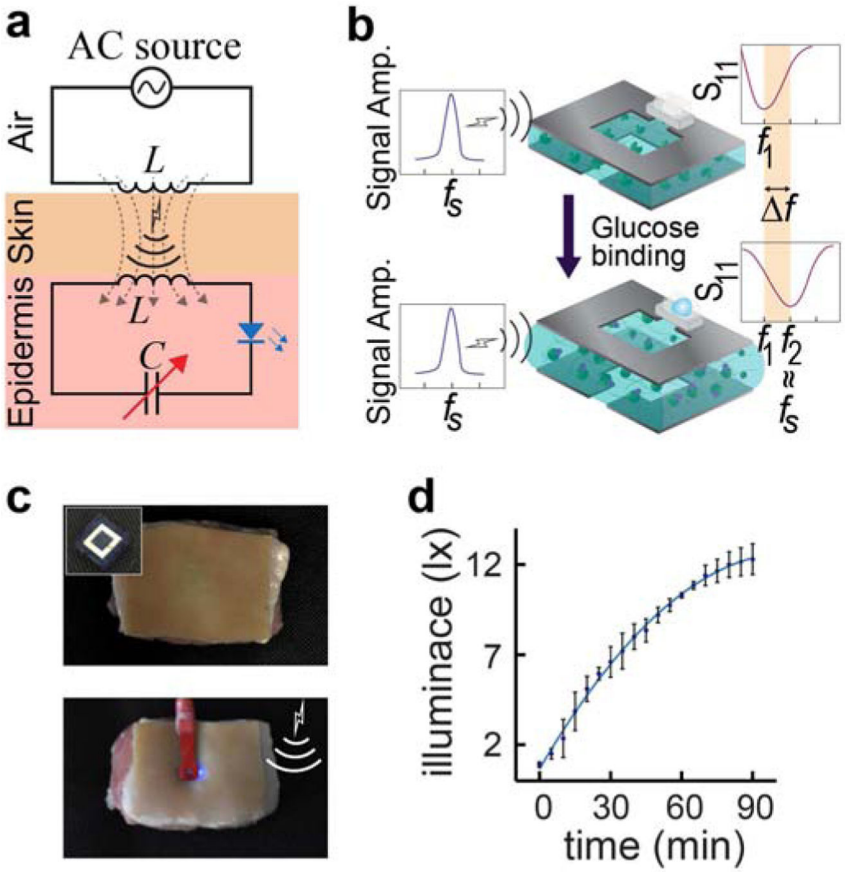


**Figure 4. Facile glucose RF reporter-tags based around glucose-dependent wireless power transfer.**

**(a)** Boronic acid-interlayer sensors are modified into glucose-monitoring RF tags via the attachment of a single LED. These tags can then be activated remotely via glucose-dependent power transfer from an active source to the RF tag via inductive coupling. **(b)** Schematic representation of the shifting of the resonant frequency of the sensor in the presence of glucose to the generating signal frequency. The more efficient power transfer to RFid sensor-circuit (due to increased glucose concentration) will increase the intensity of light emitted from the LED. **(c)** *Ex-vivo* glucose monitoring aided by wireless power transfer to an implanted RFid LED sensor under pig skin. **(d)** RF tags report on glucose concentration via intensity of light emitted from the LED (N=2, SD = 0.6 lx).

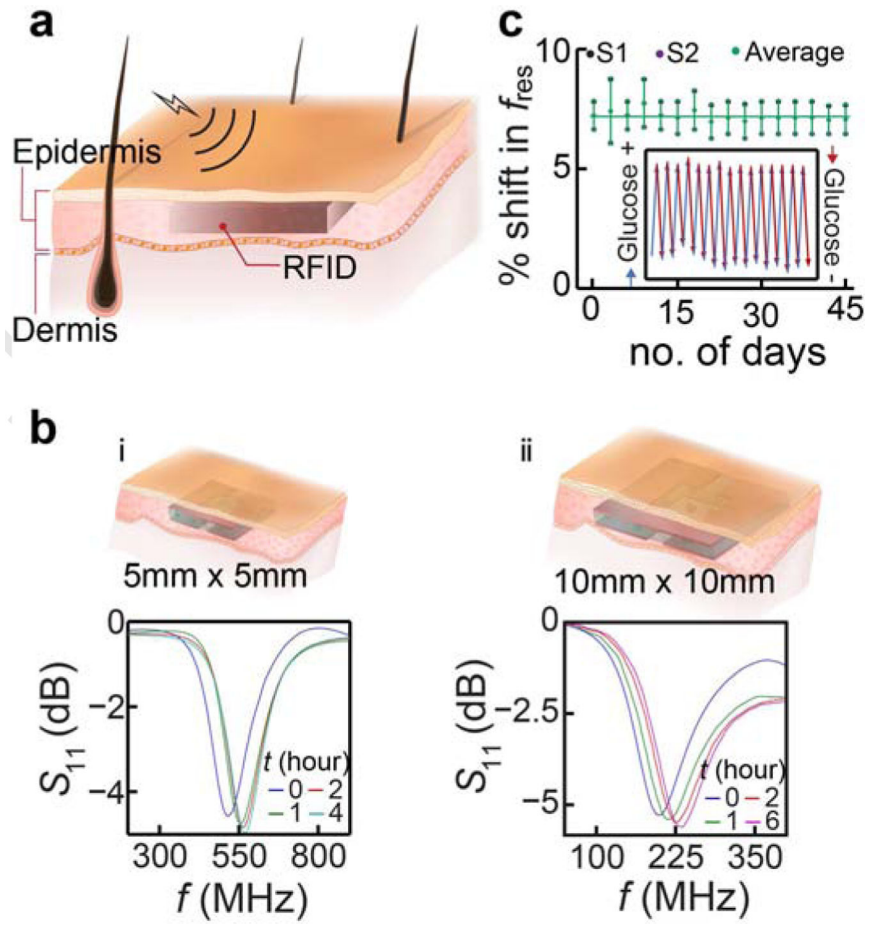


**Figure 5.** ***Ex-vivo*** **implementations and behavior of hydrogel-interlayer sensor platforms.**
**(a)** Schematic of an RF sensor implanted below the skin for continuous and long-term, passive and wireless reporting of interstitial glucose level. **(b)** *Ex-vivo* (within chicken meat) response of 25 $mm^2$ (i) and 100 $mm^2$ (ii) sensors to a set glucose concentration (500 mg/dL). **(c)** Long term (45 days at room temperature) non-degradative RF readout of the glucose sensor (N=2, SD = 5 MHz) exhibiting no signal drift/hysteresis and/or no retention of glucose in the hydrogel.